Preliminary assessment of sCO_2 cycles for power generation in CSP solar tower plants ☆

Marco Binotti *, Marco Astolfi, Stefano Campanari, Giampaolo Manzolini, Paolo Silva

Politecnico di Milano, Dipartimento di Energia, Via Lambruschini 4, 20156 Milano, Italy

This work discusses a preliminary thermodynamic assessment of three different supercritical CO_2 (sCO_2) power cycles applied to a high temperature solar tower system, with maximum temperatures up to 800 °C. The thermal power is transferred from the solar receiver to the power block through KCl-$MgCl_2$ molten salts as heat transfer fluid, therefore an indirect cycle configuration is considered assuming a surrounded field as the one of Gemasolar plant. The most promising cycle configuration in terms of solar-to-electric efficiency is selected, optimizing the cycle turbine inlet temperature to achieve the best compromise between cycle and receiver performance: the highest efficiency at design conditions is achieved by the Recompression with Main Compression Intercooling (RMCI) configuration with a solar to electric efficiency of 24.5% and a maximum temperature of 750 °C. The yearly energy yield of the proposed power plant is estimated with a simplified approach and results in the range of 18.4%: the performance decay from design to average yearly conditions is mostly due to the optical and thermal effi-ciencies reduction (−10.8% and −16.4%, respectively).

Keywords: sCO_2 cycle, Supercritical CO_2, Solar tower, Molten salts receiver, High temperature molten salts KCl-$MgCl_2$

HIGHLIGHTS

- The use of sCO2 power cycles coupled with a solar tower system is studied.
- 3 different sCO2 power cycles are optimized at different turbine inlet temperature.
- A simplified thermal model of an external solar tower receiver is developed.
- The cycles that guarantees the best solar-to-electric nominal efficiency is chosen.
- The yearly solar-to-electric efficiency for the best configuration is computed.

1. Introduction

Concentrating Solar Power (CSP) can play a fundamental role in the near future energy scenario, providing carbon-free, renewable and dispatchable electric energy to meet the increasing world energy demand. Although the Levelized Cost of Electricity (LCOE) of this technology is still non-competitive (ranging from 150 to 200 €/kWh_{el} [1]), a number of research programs is addressing its development and evolution [2,3]. Different strategies can be adopted for the reduction of the LCOE, not only related with the restraint of overnight plant costs. In fact, a reduction in the cost of electricity can be achieved also (i) through an improvement in the conversion efficiency or (ii) an increase of the equivalent operating hours of the plant by means of the adoption of a Thermal Energy Storage (TES) system. Parabolic trough (PT) can be considered the state of the art technology for CSP plants, because of the experience gained at the SEGS plants [4] and, more recently, in the United States [5] and in Spain [6–8]. However, the conversion efficiency of PT based plants is limited by the relatively low concentration factors of the collector, as well as by the usual adoption of indirect cycle configurations with synthetic oil as heat transfer fluid (HTF), whose thermal stability is limited to the upper value of 400 °C. Some attempts of using molten salts as HTF in the solar field have been made with Solar salts (60%$NaNO_3$/40%KNO_3) which allow to reach 550 °C in the solar field [9,10], but the main drawback in this case is the relatively high freezing point temperature, which poses severe technical issues to the operation of the plant in periods of absent or low sun radiation. Another promising

Article history:
Received 29 January 2017
Received in revised form 15 April 2017
Accepted 2 May 2017
Available online 5 June 2017

☆ The short version of the paper was presented at ICAE2016 on Oct 8-11, Beijing, China. This paper is a substantial extension of the short version of the conference paper.

* Corresponding author.
E-mail address: marco.binotti@polimi.it (M. Binotti).

Published Journal Article available at http://dx.doi.org/10.1016/j.apenergy.2017.05.121

Nomenclature

c_p	specific heat at constant pressure (kJ/kg-K)
E	black body emissive power (W/m^2)
h	enthalpy (kJ/kg)
J	surface radiosity (W/m^2)
k	thermal conductivity (W/m-K)
k_{is}	loading coefficient (–)
p	pressure (bar)
$\dot{Q}$	thermal power (W)
R	surface/spatial resistance (m^{-2})
SP	size parameter (m)
T	temperature (°C)
u	peripheral velocity (m/s)
V	volume (m^3)
$\dot{V}$	volumetric flow (m^3/s)
W	power (W)

Greek letters

Δ	difference
ε	effectiveness (–)
μ	kinematic viscosity (Pa s)
ρ	density (m^3/kg)

Subscript

abs	absorbed
amb	ambient
aux	auxiliaries
cl	convective losses
cycle	cycle
gr	gray
HX	heat exchange
in	inlet
int	intermediate
max	maximum
min	minimum
NET	net
out	outlet
PP	pumping power
r	refractory
tt	tube-tube
tr	tube-refractory
rad	radiative
rec	receiver
s	sky
SF	solar field
t	tube
ts	tube-sky
tot	total
y	yearly

Acronyms

ACC	air cooled condenser
CCS	carbon capture and storage
CSP	concentrating solar power
DNI	direct normal irradiation
DSG	direct steam generation
HP	high pressure
HTR	high temperature regenerator
HTF	heat transfer fluid
HVAC	heat ventilation and air conditioning
LHV	lower heating value
LCOE	levelized cost of electricity
LP	low pressure
LTR	low temperature regenerator
PC	partial cooling
PCHE	printed circuit heat exchanger
PT	parabolic trough
RMCI	recompression with main compression intercooling
RPM	rounds per minute
RPR	recompression pressure ratio
RR	recompression
ST	solar tower
TES	thermal energy storage
TIT	turbine inlet temperature

technology could be based on linear Fresnel reflector [11,12], whose strength is mainly related to the simplicity of construction and theoretically low costs, together with the possibility to implement direct steam generation (DSG) plant configurations. However, their cost reduction capability is still to be demonstrated and the annual energy yield of the plant is strongly penalized by poor average optical efficiency [13].

Among the different CSP technologies, solar towers (ST) are considered as the most promising in terms of potential LCOE reduction [2] thanks to the high potential concentration ratio (typically from 500 to 2000), which leads to higher maximum temperatures and more efficient thermodynamic conversion power cycles. Nowadays, about 430 MW_{el} of commercial ST plants are operating (mainly in Spain and US), while other 430 MW_{el} are under construction in China, US, Chile and South Africa and other 1500 MW_{el} are in the planning phase [14]. All the ST currently in operation are based on traditional Rankine steam cycles for the conversion of the thermal power.

Supercritical carbon dioxide (sCO_2) cycle has been identified by key international energy stakeholders [2,15–19] as a promising technology to increase flexibility and efficiency. Compared to steam Rankine cycle, this type of closed Brayton cycles have smaller weight and volume, lower thermal mass and less complex power blocks due to the higher density of the fluid and simpler cycle design [20]. Supercritical CO_2 cycles have been proposed for different applications and thermal sources (coal, biomass, solar, etc.). Dealing with conventional sources, sCO_2 cycles for coal fired power plants have been investigated, showing theoretical performance up to 47.8% LHV efficiency, employing existing materials at current operating conditions [16]. Moreover supercritical CO_2 cycles for nuclear reactors have been deeply analyzed, showing the capability of reaching high efficiency, while still retaining simplicity [21,22].

Although most of the studies have considered so far sCO_2 for nuclear power plants, there is a growing interest in deploying them in CSP applications [23–25]. Supercritical CO_2 cycles coupled with high temperature solar receivers are recognized to be a promising technology to reduce investment costs and at the same time increase the conversion efficiency [26,27]. Supercritical CO_2 based Brayton cycles have been compared with trans and sub-critical working conditions of the same fluid, highlighting their advantage in terms of efficiency and extremely small volumetric flow rates, resulting in a compact design [28]. Supercritical CO_2 cycles in CSP plants have been considered in indirect configuration, evaluating their response in terms of flexibility and part-load performances [26]. Flexibility features can take advantage of the lower heat capacity of the turbomachinery that enables faster start-ups and load variations, easier start-up/shut down operations and wider load operating range than a conventional steam-based cycle. Dynamic response of a recompression-cycle configuration has been

also addressed in a solar tower with a direct configuration [29]. Supercritical CO_2 cycles have been also proposed coupled to parabolic trough solar fields in a direct configuration, however in this case their dynamic behavior is related to the collector and poses severe mechanical and control issues [30].

The main challenges of sCO_2 application, especially coupled to CSP plants, are heat exchanger design and material selection [18], as well as high pressure conditions. Regarding materials, protective barriers with stable oxides (chrome and nickel, and alumina) or steel alloys with high concentrations of chromium and nickel have been proposed in sCO_2 power cycles to increase resistance to high temperature corrosion [31,32]. On the other hand, considering high pressure concerns, it can be pointed out that indirect configurations with a HTF offer the advantage of low pressures inside the solar receiver with better dynamic response of the system to the severe transient conditions which CSP plants are often exposed. In addition to this, it is worth noting that thermal storage integration is easier with an indirect configuration.

In this work, a preliminary thermodynamic assessment of three different sCO_2 power cycles, exploiting heat collected in a high temperature solar tower system is carried out. The maximum investigated sCO_2 temperature is set at 800 °C. An indirect cycle configuration is assumed, where KCl-$MgCl_2$ molten salts mixture is used as HTF in the solar receiver, allowing for a lighter and cheaper receiver design with respect to the case of a high pressure direct sCO_2 receiver and allowing an easier TES integration. The most promising cycle configuration is selected, optimizing the Turbine Inlet Temperature (TIT) to achieve the best compromise between cycle and receiver efficiency. An estimate of the yearly energy yield of the proposed power plant is also performed. To the authors' knowledge, there are no papers available in literature which assess the solar-to-electric efficiency of advanced solar tower plants including innovative fluids and sCO_2 cycles both at design and on yearly base conditions. The results of this work can indicate where to point the R&D attention for further developing CSP technology.

2. Design performance

2.1. Power cycle

Three different regenerative sCO_2 power cycles, following the lay-out previously discussed in literature [20,21,33] were investigated and modeled using Excel and Refprop [34]. The three selected options are Recompression (RR), Partial Cooling (PC) and Recompression with Main Compression Intercooling (RMCI) cycles. These plants layouts are the most promising for high temperature solar applications and it has been demonstrated that they could achieve higher efficiency with respect to the simple recuperative cycle that suffers real gas effects on the recuperator high pressure side at low temperature: the increased sCO_2 specific heat capacity with respect to the low pressure side of the regenerator leads to large temperature differences and thus to heat exchange irreversibilites.

The RR plant aims to reducing this efficiency loss splitting the fluid mass flow rate before the heat rejection unit: one fraction is directly compressed up to the maximum pressure of the cycle while the other is cooled down releasing heat to the environment before entering the main compressor. The streams are mixed again after the second compressor and the mixed flow rate enters at first a high temperature recuperator and then the primary heat exchanger. A proper choice of the split ratio allows to balance the hot and cold fluid heat capacities and to minimize the temperature differences in the heat transfer process. The PC layout is similar to the previous one with the difference that an additional compressor and cooler have been added. Moreover, the minimum cycle pressure can be selected lower than the critical pressure. This allows increasing the expansion pressure ratio and possibly the plant productivity. The last option is the RMCI plant which is basically the RR plant with an intercooled compression in order to better exploit the real gas effects and reduce the compression work. In all the cycles the sCO_2 streams exiting the cold side of the low temperature regenerator and the intermediate compressor have the same temperature to minimize mixing irreversibilities [20].

The performance of the three cycles as function of the TIT were determined, setting 250 bar as turbine inlet pressure and maximizing cycle efficiency as function of the minimum cycle pressure and of the intermediate pressure level (for PC and RMCI) defined by the Recompression Pressure Ratio (RPR) parameter:

$$RPR = \left(\frac{p_{max}}{p_{int}} - 1\right) \Big/ \left(\frac{p_{max}}{p_{min}} - 1\right) \quad (1)$$

Apart from the primary heat exchanger where heat is transferred from the HTF to the CO_2, the three sCO_2 power cycle layouts are basically made by two types of heat exchangers (the regenerator(s) and the heat rejection unit(s)) and two turbomachinery (the compressor(s) and the turbine). Various studies have been carried out in past years about the design [21,35] and optimization of these components while various ongoing experimental activities are focused to the construction of prototypes and test in a relevant environment [15,36–38].

In the heat rejection unit(s) the CO_2 is cooled down after the regenerator and after the first compression stage in PC and RMCI configurations by means of air coolers. These components can be designed as conventional gas coolers where the hot CO_2 stream is distributed in a number of finned tubes arranged in different ranks while air is sucked or blown by fans flowing in crossflow with respect to the tubes bank. This kind of technology is already used in Heat Ventilation and Air Conditioning (HVAC) field with CO_2 maximum inlet conditions around 150 °C and 120 bar [39] (namely thermodynamic conditions more severe than in our optimized case). Fan consumption depends on (i) heat exchanger architecture (frontal area, number of ranks, tube disposition, fins type and spacing), (ii) air mass flow rate and (iii) ambient temperature: a pressure drop of 2% on the tube side and an electrical fan consumptions ($W_{aux,PB}$) equal to 1.25% of the rejected heat at the ambient temperature of 40 °C were assumed as reference value, according to a preliminary design of the required air coolers obtained by a manufacturer [40].

More challenging is the design of the regenerator(s) because of the low overall heat transfer coefficient and the very high pressure difference between the cold and the hot side. In the design of this component it is crucial to adopt compact solution in order to reduce the footprint, the cost and the thermal inertia. Different types of heat exchangers are proposed in literature [36]: shell&tube, brazed or bonded plate heat exchangers and printed circuits heat exchangers (PCHE). The first architecture is strongly penalized by a large footprint, the lowest thermal efficiency, high thermal inertia and vibration issues while the others are very compact but tend to lead to higher pressure drops because of the small hydraulic diameters. The last configuration is one of the most promising for this type of application because it can operate at very high pressures: metal flow plates are manufactured by chemical etching of 1.6 mm thick metal plates, forming complex flow patterns and thin passages (e.g. 2 mm diameter semi-circles), in order to increase the heat transfer coefficient. Finally, metal flow plates are stacked and diffusion-bonded at high temperature and pressure, forming a high-integrity solid block with multiple flow channels. One of the main manufacturers [41] claims that bonded PCHE can be 80% smaller than a conventional heat exchanger and

operate up to 965 bar and 980 °C. In the plant optimization we assumed a constant relative pressure drop and a fixed effectiveness for the regenerators. Pressure drops are higher on the low pressure side (1.5%) with respect to the high pressure side (1%), according to the larger volume flow rate. The effectiveness of the low temperature regenerator (93%) is slightly lower than for the high temperature regenerator (95%) because in the first component the balance of heat capacity of hot and cold streams already allows to minimize the irreversibility due to heat transfer.

From the turbomachinery side, the high molecular mass of CO_2 and the very high pressures in the cycle allow designing compact machines with a limited number of stages and a small size (i.e. mean diameters), reducing the turbomachinery cost. The compressor has a particular design since it works close to the critical point in a region with significant real gas effects: the volumetric behavior of CO_2 sharply changes during compression and the optimization of the blade profile is a non-trivial issue. In spite of these peculiarities sCO_2 compressors are already available on the market and they are mainly developed in the oil and gas industry (e.g. for enhanced oil recovery with CO_2 pressurization for transport and injection in oil reservoirs) as well as for future CCS applications. Either radial compressors or axial compressors can be used, depending on the plant size, with maximum operating pressure around 250 bar as claimed by manufacturers.

The turbine design can benefit from limited real gas effects and a small volumetric flow variation, but it faces issues related to small size that inevitably leads to high secondary losses and a higher weight of leakage losses across the stator-rotor clearance, thus jeopardizing the efficiency. For the purpose of this parametric analysis, according to a numerical correlation given in [42], the turbine efficiency was varied as a function of the volume ratio *VR* and of the size parameter *SP* (a quantity strongly related to turbine radial dimension), defined as:

$$VR = \frac{\dot{V}_{out,is}}{\dot{V}_{in}} \tag{2}$$

$$SP = \frac{\sqrt{\dot{V}_{out,is}}}{h_{is}^{1/4}} \tag{3}$$

The volumetric flow at the expander outlet at isentropic conditions $\dot{V}_{out,is}$ depends on the sCO_2 mass flow in the primary heat exchanger, thus it is computed iteratively as a function of the receiver efficiency. A detailed turbine study was subsequently carried out for the most promising cycle configuration (see Section 3.1). In Fig. 1 a graphical overview of the solar tower plant and of the three sCO_2 cycles with the corresponding T-s diagrams is reported, while Table 1 summarizes the main design assumptions.

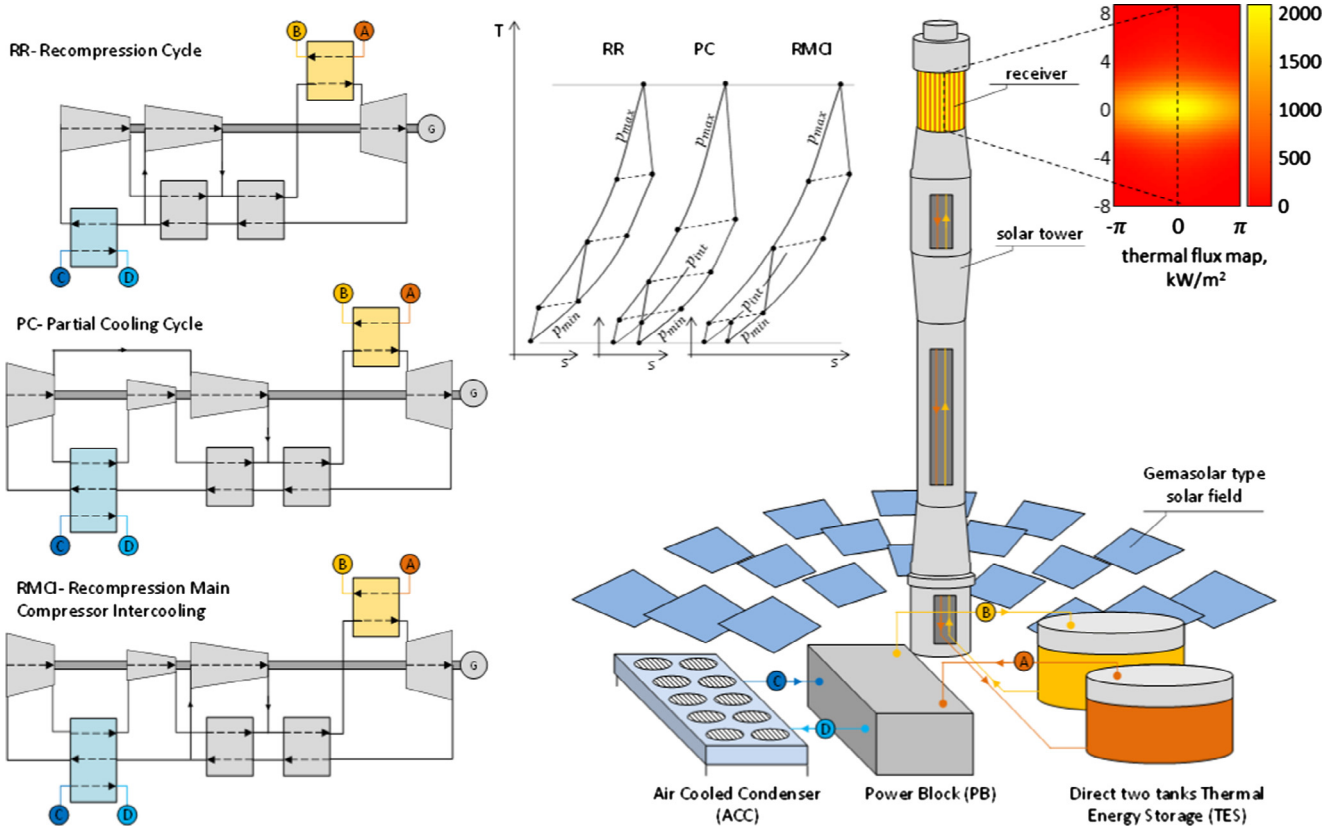

Fig. 1. Investigated sCO_2 cycles layouts and overall system schematic.

Table 1
Main assumptions for the power cycle simulation.

Parameter	Value	Parameter	Value
Turbine inlet pressure (bar)	250	$\Delta p/p$ primary Heat Exchanger	0.015
Minimum temperature (°C)	51	$\Delta p/p$ heat rejection Heat Exchanger	0.02
LTR/HTR effectiveness, ε	0.93/0.95	Compressor isentropic efficiency	0.89
$\Delta p/p$ HP/LP side of regenerator	0.01/0.015	Mechanical/Electrical efficiency	0.99/0.99

2.2. Tower and receiver

The solar field and the receiver geometry were assumed similar to the one of the Gemasolar plant, consistently with previous works [43–45]: the surrounded solar field consists of 2650 canted heliostats of 110 m^2 each, concentrating the solar radiation onto a tubular external receiver with a diameter of 8 m and 16 m high. The Solar Multiple is 2.8 and the Thermal Energy Storage (TES) consists of a direct two-tanks system with a capacity of 13 equivalent hours.

The nominal optical efficiency and the heat flux map on the receiver were computed with DELSOL3 [46] assuming a DNI of 970 W/m^2 and solar noon on the summer solstice (June 21st) as reference day and time for the selected site (Sevilla, 37°42′N, 5°9′W, DNI_y = 2090 kWh/m^2-y). The calculated optical efficiency, equal to 68.3%, is determined assuming for simplicity all the heliostats aiming at the equator of the receiver [43] leading to the highest optical efficiency together with the highest peak temperature on the tubes. The main geometrical parameters of the receiver are reported in Table 2 while the design heat flux map is shown in Fig. 1.

A preliminary screening of potential HTFs was performed among the molten salts that (i) are chemically stable and liquid up to 800 °C, (ii) have solidification temperature below 525 °C and (iii) are compatible with high-temperature alloys. In this preliminary selection, HTF cost, required pumping power (PP) and heat transfer characteristics (HX) were evaluated and compared. The last two aspects were taken into account as suggested in [47], through the calculation of two non-dimensional figures of merits (*FOM*) which are reported here:

$$FOM_{PP} = \frac{\mu^{0.2}}{\rho^2 c_p^{2.8}} \tag{4}$$

$$FOM_{HX} = \frac{\mu^{0.2}}{\rho^{0.3} c_p^{0.6} k^{0.6}} \tag{5}$$

The most suitable HTF and storage media is KCl-$MgCl_2$, a mixture of salts whose main characteristics are reported in Table 3. This type of salt can withstand temperatures up to 800 °C. Therefore, the selected material for the receiver tubes was INCOLOY 800 HT, a nickel-based alloy widely applied in the chemical industry for its excellent corrosion resistance as well as strength at high temperatures, which is considered to be a good candidate for this application. Nevertheless, further investigation and detailed studies should be carried out to verify the long-term chemical stability of the tube material vs. the selected salts.

A simplified thermal resistance model [48] adapted from [49] was implemented in Matlab and used for the evaluation of the receiver thermal losses. The model estimates the convective losses through literature correlations [50,51] and applies an equivalent electric resistance network to compute the radiative losses. The equivalent electric resistance network is reported in Fig. 2. Each panel is discretized in vertical segments and the energy balance, reported in Eq. (6), is subsequently solved for each tube segment, starting from the HTF inlet and following the HTF flow through the panels of each flow path.

$$\dot{m}_{HTF,t} c_{p,HTF} T_{HTF_{in}} + \dot{Q}_{abs,t} = \dot{m}_{HTF,t} c_{p,HTF} T_{HTF_{out}} + \dot{Q}_{cl,t}(T_w) + \dot{Q}_{rad,t}(T_w) \tag{6}$$

The model was initially tested for the Gemasolar operating temperatures (290–565 °C), with Solar Salts (60%$NaNO_3$/40%KNO_3) as HTF. Although no performance data are available for the Gemasolar receiver, the obtained thermal efficiency of 86.01% appears to be in the range of efficiencies reported by similar works [49,52]. For the present study, the thermal performance of the receiver as function of the TIT was computed assuming a constant ΔT of 15 °C between the selected salts and the sCO_2 maximum temperature in the primary heat exchanger. The ambient temperature was set at 30 °C and the wind speed at 4 m/s.

The performance obtained with the simplified thermal model are reported in Table 4 for a case using KCl-$MgCl_2$ molten salts and compared to the Gemasolar Case. The receiver power balance with KCl-$MgCl_2$ was determined assuming the temperatures obtained for a RMCI cycle with maximum TIT of 750 °C (see Section 3.1).

The higher average and maximum temperatures of the receiver strongly influence the radiative and convective losses, reducing the receiver efficiency with respect to Solar Salts of about 11%. It is also possible to notice how the required HTF mass flow is strongly increased (by nearly 50%) for KCl-$MgCl_2$ molten salts due to their lower ΔT across the receiver and their lower specific heat. A rigorous analysis should consider an optimized number of flow paths in the receiver as a function of the molten salts ΔT and mass flow rate; however, the effect of a different flow paths arrangement on the receiver efficiency is limited, as reported in [53], and thus a fixed number of flow paths was here considered for simplicity. On the contrary a more important variation can be expected for the molten salts circulation pumping power ($W_{aux,SF}$): thus, calculation

Table 2
Main characteristics of the ST receiver for a Gemasolar type plant.

Parameter	Value	Parameter	Value
Receiver height above ground (m)	116	Number of panels	16
Receiver Diameter, m	8	Number of tubes per panel	38
Receiver Height, m	16	Tube external diameter, m	0.0395
Number of flow path	2	Salts pump overall efficiency	0.75

Table 3
Main characteristics of the selected molten salt.

Parameter	Value	Parameter	Value
Molar Composition	67%KCl/33%$MgCl_2$	Viscosity @ 700 °C (cP)	1.44
Solidification temperature (°C)	426	Thermal conductivity @ 700 °C (W/m-K)	0.39
Boiling temperature (°C)	> 1418	FOM_{PP} (forced convection, turbulent)	5.66
Density @ 700 °C (kg/m^3)	1593	FOM_{HX} (heat exchanger area)	39.7
Specific Heat @ 700 °C (kJ/kg-K)	1.1555	Estimated Cost (€/kg)	0.26

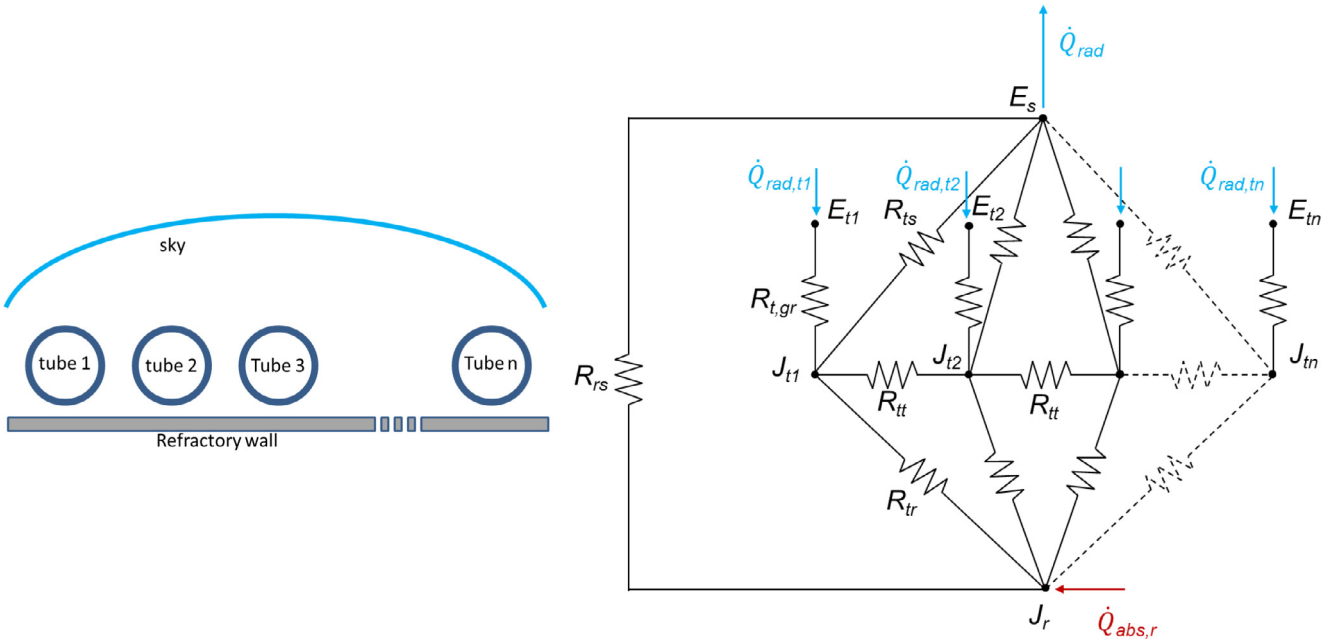

Fig. 2. – (Left) Schematic of the surfaces involved in the radiative heat exchange in a solar receiver panel and (Right) corresponding electric resistance model. For simplicity a panel with four tubes is represented.

Table 4
Main results of the simplified receiver thermal model with standard "Solar salts" and with the selected molten salts.

	Gemasolar Case	High temperature receiver
HTF type	60%$NaNO_3$/40%KNO_3	67%KCl/33%$MgCl_2$
$T_{in,\ HTF}$ (°C)	290.0	554.7
$T_{out,\ HTF}$ (°C)	565.0	765.0
HTF Mass Flow (kg/s)	396.4	606.9
Thermal Efficiency (%)	86.01%	76.48%
Max Wall Temperature (°C)	663.7	855.6
Convective Losses (MW)	4.06	6.68
Radiative and Reflective Losses (MW)	22.8	38.51

was performed assuming the same mass flow rate per tube of the Gemasolar case and taking into account also the tower height.

3. Design condition results

This section summarizes the performance of the three selected sCO_2 configurations at design conditions (summer solstice, solar noon). The receiver thermal efficiency and the corresponding HTF inlet temperature, the cycle gross efficiency and the system net power ($W_{NET} = W_{cycle} - W_{aux,SF} - W_{aux,PB}$) are reported in Fig. 3 for the three cycles as function of the TIT: it is possible to highlight the contrasting effects of the TIT on the cycle efficiency and the receiver thermal efficiency resulting in a maximum power output for each investigated plant. The higher the TIT, the higher is the cycle gross efficiency, but receiver thermal losses increase because of the higher average receiver temperature. Therefore, there is a TIT which maximizes the electric power output; this condition also brings about the maximum solar-to-electric efficiency because all cases are operating with the same solar field and thus with the same optical efficiency.

Detailed power balances of the three cases at their maximum efficiency point and the corresponding values of minimum cycle pressure and RPR are reported in Table 5.

A maximum net electric power of about 24.8 MW_{el} was obtained by the RMCI cycle for a TIT temperature of 750 °C, with a corresponding solar to electric efficiency of about 24.5%. The receiver thermal efficiency in the same point is 76.5%, with molten salts rising their temperature in the receiver from 555 °C up to

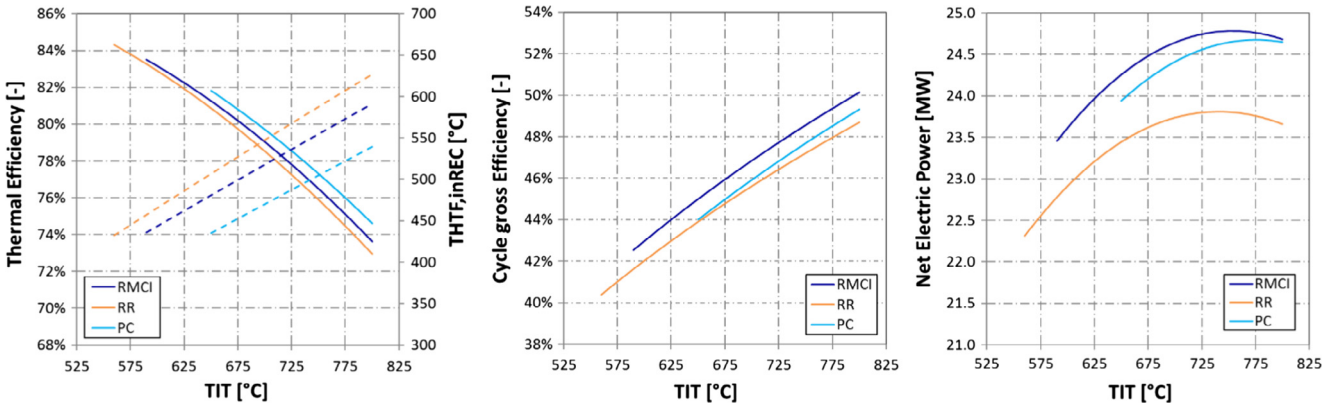

Fig. 3. (Left) Receiver efficiency, (Center) Cycle Gross efficiency and (Right) net power of the three investigated cycles layouts as function of the TIT.

Table 5
Main results for the three different studied power cycles.

Parameter @ maximum efficiency	PC	RR	RMCI
Optimum TIT (°C)	780	740	750
Minimum cycle pressure (bar) @ optimum TIT	5.23	9.37	7.06
RPR @ optimum TIT	0.356	–	0.548
Available Solar power (MW)	282.8	282.8	282.8
Thermal power at the receiver (MW)	193.1	193.1	193.1
Thermal power to the HTF (MW)	146.2	147.6	147.7
Receiver thermal losses (MW)	46.9	45.5	45.4
Thermal power to power block, SM = 1 (MW)	52.2	52.7	52.8
Power block gross power output, SM = 1 (MW)	25.42	24.73	25.62
Auxiliaries consumptions, SM = 1 (MW)	0.74	0.92	0.83
Net power output, SM = 1 (MW)	24.68	23.81	24.78

765 °C; with a minimum approach point temperature difference set to 15 °C in the HTF-CO_2 heat exchanger, this ensures the TIT of 750 °C for the power cycle, running with a cycle gross efficiency of about 48.6%. The RMCI cycle with a TIT of 750 °C was thus selected for the yearly simulation.

3.1. Turbomachinery design

The turbine design must be optimized in order to achieve high efficiency. A dedicated numerical tool [54] was used to verify the performance of the expander, in order to obtain a preliminary stages design and to optimize the rotational speed: the results related to the optimal plant are here discussed. The numerical tool is designed to optimize multistage axial turbines including real gas effects and it based on pseudo-1D approach. It uses a different efficiency loss correlations derived from literature and based on the experimental works of Craig and Cox [55] and Kacker and Okapuu [56] to determine a reliable expansion efficiency of each turbine row. As result the overall total-to-static efficiency is computed taking into account the actual blade geometry and the presence of supersonic flows. The main parameters of interest for the design of the expander are V_r and the isentropic enthalpy drop across the expander Δh_{is} for the optimal configuration they are respectively equal to 2.64 and 219.6 kJ/kg. The speed of sound varies from around 480 m/s at turbine inlet and 440 m/s at turbine outlet, thus a first solution could be to manage the whole expansion in a single stage with relatively low loading coefficients ($k_{is} = \frac{2\Delta h_{is}}{u^2}$) and a peripheral speed below 450 m/s Because of the small volumetric flow rate, the optimal rotational speed is quite high and is optimized at 30,000 RPM. Mean diameter results to be 26 cm with a peripheral speed of 414 m/s and the stage has a high degree of reaction (0.415). Overall isentropic efficiency is 89.04%, mainly penalized by secondary losses (related to the small blade heights), tip leakage losses (because of the large relative radial gaps) and marked profile losses due to the thickness of blade trailing edge. Slightly supersonic velocity is obtained at stator outlet, with post expansion after the converging nozzles. Better results can be achieved by a solution employing a two stage turbine rotating at 24,000 RPM and with a three-stages turbine with a rotational speed equal to 19,000 RPM.

Fig. 4 depicts the blade geometry (rotor and stator) in a meridian plane and the velocity triangles reported in terms of Mach numbers for a single stage, a two stage and a three stage turbine while Table 6 reports turbines main characteristics. Increasing the number of stages allows reducing the enthalpy drop for each stage thus limiting the peripheral speed and the rotational speed of the turbine. Repartition of enthalpy head leads also to lower Mach numbers with subsonic velocity triangles. In multistage turbines the mean diameter slightly decreases and the first stage blade height is kept at reasonable values by the possibility to choice a proper value for the first stage loading coefficient and thanks to the smaller velocities in axial direction. This reflects in almost unchanged secondary and corner losses while kinetic energy loss at turbine discharge are reduced. As results, higher is the number of stages, higher the efficiency that is 90.64% and 91.13% for the two stage and the three stage turbine respectively. Using a more expensive four stage turbine would probably lead to a further increase of efficiency but considering the efficiency trend obtained the margin of improvement is limited and so a three stage turbine is suggested for this case. The calculated value of isentropic efficiency for the three stage turbine is consistent with the values obtained with the numerical correlation mentioned in Section 2.1 for the cycle optimization routine.

It is important to highlight that regardless of the turbine number of stages a high rotational speed must be used to achieve high efficiency, thus not allowing a direct coupling of the electric generator with the grid and requiring the use of a gearbox or a power electronic system to adapt the power generation frequency.

3.2. Sensitivity analyses

With respect to the obtained results, two sensitivity analyses were performed for the RMCI case in order to evaluate the effects

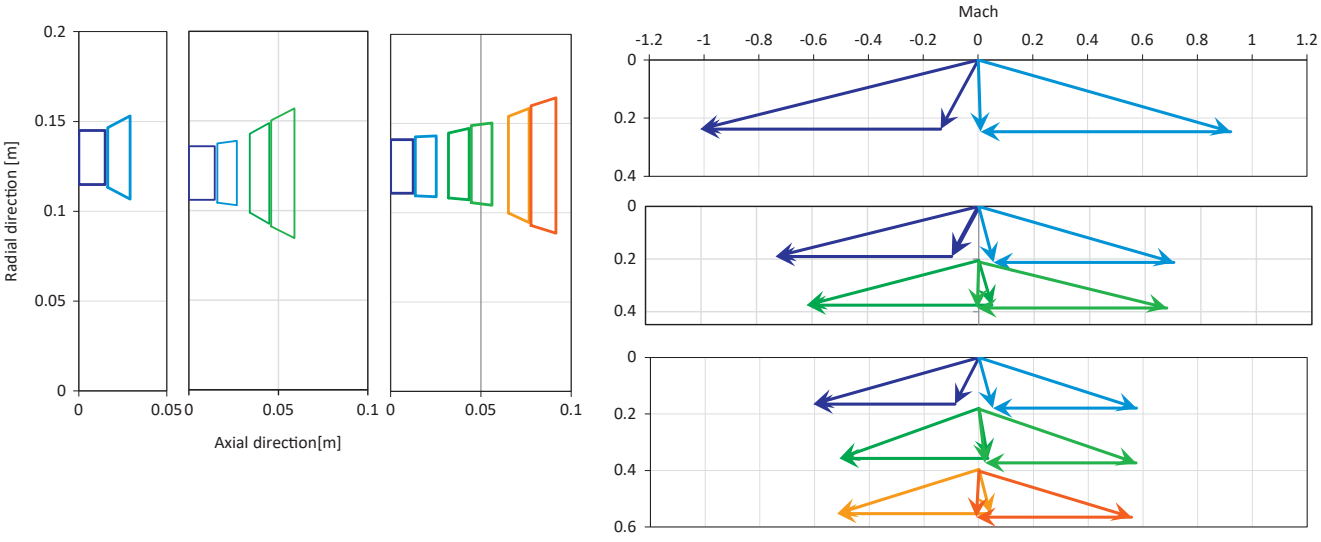

Fig. 4. (Left) Radial profiles e and (Right) velocity triangles (reported in terms of Mach number) for single stage, two-stage and a three-stage turbine.

Table 6
One, two and three-stage turbine design results for the optimum RMCI cycle.

	Single stage	Two-stage		Three-stage		
Optimal rotational speed (RPM)	30,000	24,000		19,000		
Efficiency (–)	89.04%	90.64%		91.13%		
Pheripheral speed (m/s)	414	303		260		
Mean diameter (m)	0.26	0.24		0.26		
Blade height 1st stage (m)	0.032	0.03		0.03		
Exit velocity (m/s)	107	81		71		
		1st	2nd	1st	2nd	3rd
Stage loading coefficient (–)	2.56	2.92	2.03	2.76	2.04	2.02
Degree of reaction (–)	0.414	0.446	0.510	0.325	0.48	0.50
efficiency stage, total-to-total (–)	90.2%	90.1%	91.8%	89.7%	91.6%	92.4%
VR	2.64	1.74	1.56	1.45	1.35	1.38
SP (m)	0.095	0.088	0.119	0.088	0.110	0.130

of some of the made assumptions. In particular, the impact of the high temperature regenerator (HTR) effectiveness and the effect of an increase of the receiver efficiency were evaluated.

The effectiveness of a heat exchanger is a parameter directly related to the minimum temperature difference (ΔT_{pp}) in the heat exchanger and it is defined as the ratio between the actual heat exchanged $\dot{Q}$and the maximum possible heat exchanged obtainable with an infinite heat exchange area $\dot{Q}_{\infty}$ ($\Delta T_{pp} = 0$). For the HTR this can be computed as:

$$\varepsilon_{HTR} = \frac{\dot{Q}}{\dot{Q}_{\infty}} = \frac{h(T_{in,LP}, p_{in,LP}) - h(T_{out,LP}, p_{out,LP})}{h(T_{in,LP}, p_{in,LP}) - h(T_{in,HP}, p_{out,LP})} \quad (7)$$

where $T_{in,LP}/T_{out,LP}$ and $p_{in,LP}/p_{out,LP}$ are the inlet/oultet temperatures and pressures of the hot low pressure sCO_2 stream in the HTR and $T_{in,HP}$ is the inlet temperature of the cold high pressure sCO_2 stream in the HTR. An effectiveness of 0.95 for the best performing RMCI cycle (TIT = 750 °C) corresponds to ΔT_{pp} = 17.3 °C at the cold end temperature side of the HTR. A lower effectiveness reduces the heat exchanged in the HTR as well as the heat exchanger area and thus its cost. In terms of efficiency, a lower effectiveness has a detrimental effect on the cycle efficiency, but, on the other hand, reduces the inlet temperature in the primary heat exchanger and thus the molten salts temperature in the receiver with advantages in terms of thermal losses. With respect to the reference effectiveness of 0.95, two cases with ε_{HTR} = 0.98 and ε_{HTR} = 0.90 that correspond to a ΔT_{pp} in the HTR of about 8.5 °C and 30.7 °C respectively were evaluated. Results reported in Fig. 5 indicate that in the trade-off between receiver and cycle efficiency, the latter is predominant hence the gross power is lower at lower effectiveness.

Due to the difficulty of benchmarking the receiver efficiency with experimental data and due to the large dispersion of data available in literature, a further case with enhanced receiver efficiency was also studied. For simplicity, a 15% reduction in the receiver thermal losses is assumed and the calculated results are reported in Fig. 5. The higher thermal efficiency leads to an overall net power increase of about 5.3% achieved at TIT equal to 780 °C.

4. Yearly results

The yearly simulation was performed on hourly basis using DNI and ambient temperature data available in [57] for the chosen site. The optical efficiency as function of Azimuth and Zenith is the same reported in a previous work [58] and obtained with DELSOL 3. The receiver thermal efficiency, which is function of both the solar power hitting the receiver $\dot{Q}_{rec}$ and of its distribution on the receiver, was computed for nine different sun positions in order to limit the computational time. A schematic of the nine different sun positions used for the evaluation of the thermal efficiency is reported in Fig. 6, left: the N-S solar field and receiver symmetry lead to symmetric maps around solar noon. In Fig. 6, right, the thermal efficiency for the nine selected sun position is computed as function of the incident solar power: results show that the influence of the sun position and thus of the flux distribution is limited, while the effect of the overall incident solar power is the most significant one. In the annual simulation, the hourly thermal efficiency was thus computed as function of the incident solar power choosing the nearest flux distribution among the nine selected (i.e. one among the nine curves reported in Fig. 6).

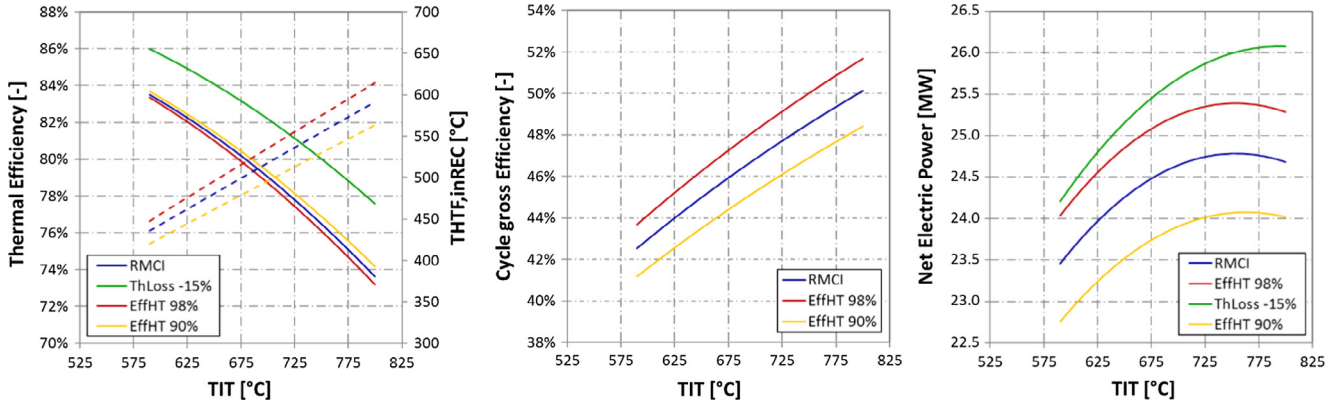

Fig. 5. (Left) Receiver efficiency, (Center) cycle gross efficiency and (Right) net electric power for the RMCI case with the assumptions of Table 1 (blue line), with increased/reduced regenerator effectiveness (red and yellow lines) and with reduced receiver thermal losses (green line). (For interpretation of the references to colour in this figure legend, the reader is referred to the web version of this article.)

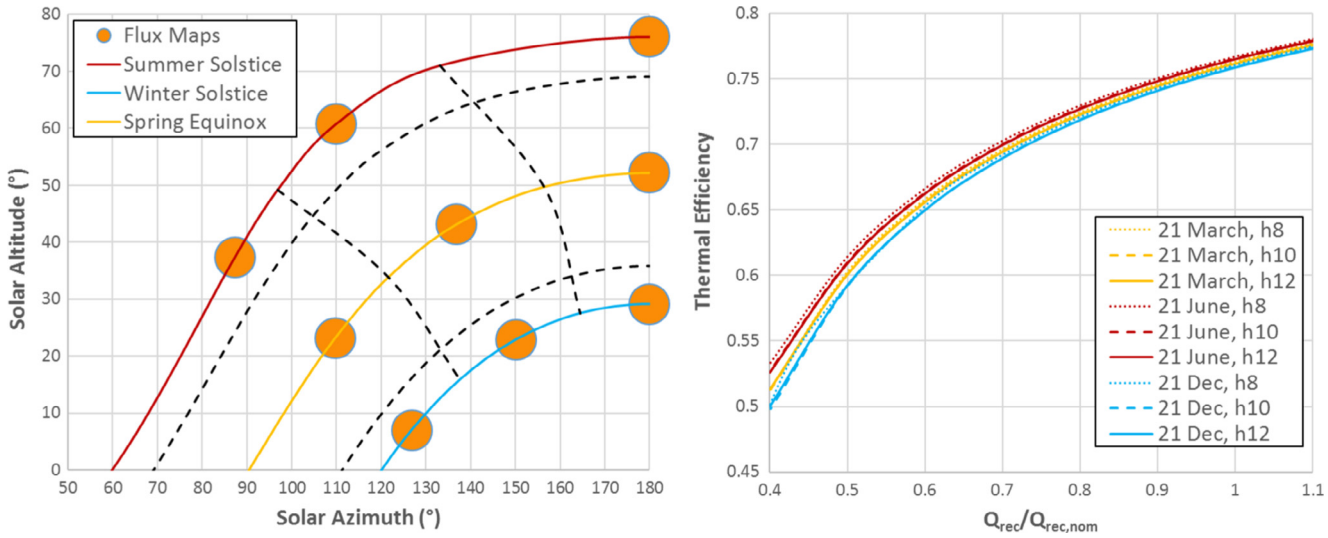

Fig. 6. (Left) Nine flux reference maps and selection procedure and (Right) thermal efficiency as function of the incident thermal power on the receiver for the nine reference maps.

Table 7
Yearly results for the RMCI case (in brackets the nominal efficiency values).

Parameter	Value	Parameter	Value
Yearly optical efficiency (%)	60.95 (68.3)	Yearly solar field aux efficiency (%)	97.66 (97.68)
Yearly thermal efficiency (%)	63.91 (76.48)	Yearly solar-to-electric efficiency (%)	18.38 (24.46)
Yearly net PB efficiency (%)	48.31 (47.93)	Yearly net electric energy (GWh)	111.95

Assuming a large TES size similar to the one of the Gemasolar (13 h), allows the power block to operate at nominal molten salt mass flow rate throughout the entire year. The minimum cycle temperature and pressure are also kept constant assuming a variable consumption of the heat rejection system. Fan consumption is calculated as a function of ambient temperature based on their nominal power computed at 40 °C ($W_{aux,PB,40}$) according to the following correlation obtained from preliminary design of the required dry coolers [59]:

The equation reflects the reduction of ventilation power when the ambient temperature decreases and a lower air flowrate and number of fans is required to draw heat from the cooler. In all cases, the power consumed by the fans remains below 1% of the turbine gross power.

The molten salts pumping power was determined for every hour taking into account the HTF flow variation. The yearly results for the RMCI case are reported in Table 7, according to the efficiencies chain, as suggested in [13]. The yearly solar-to-electric efficiency of 18.4% is comparable with the one that was obtained for a standard Gemasolar type plant (18.8%), underlying how the advantages in terms of PB conversion efficiency (48.31% vs 39.07% [44]) are counterbalanced by the lower receiver thermal performance (63.91% vs 80.00%). As already pointed out, it must be outlined that these results are obtained assuming a solar field and concentration ratios which are optimized for classic solar salts operating conditions. When using different HTF (as in this case) or power cycle it would be required to take into account in the overall optimization also the heliostat field design (i.e. number of heliostat and their size and position). A higher concentration ratio can be necessary when operating at high temperatures (up to 800 °C as in this work) to increase the thermal efficiency of the receiver in particular at off-design conditions. However, a higher concentration ratio or the operation with higher peak fluxes on the receiver can imply the use of a different heat transfer fluid with higher heat transfer properties (i.e. liquid metal). The use of such HTFs would allow peak flux double with respect to molten salts [60], halving the receiver area and thus thermal losses. Summarizing, the finding that the yearly solar electric efficiency of the sCO_2 configuration with high temperature molten salts is slightly lower with respect to the case of a steam cycle with conventional solar salts does not mean that the technology is not worth investigating. On the contrary, it has significant potentiality because results are achieved with heliostat field and receiver designed and optimized for another technology (i.e. for standard solar salts with steam cycle). Finally, the power block of sCO_2 cycles can be significantly cheaper than for conventional steam cycles, therefore, potentially reducing the solar plant capital costs [21,25,26].

5. Conclusions

This work discusses a preliminary assessment of different sCO_2-power cycles applied to high temperature solar tower systems, with maximum temperatures up to 800 °C. The analysis performs an energy analysis of a solar tower plant based on indirect cycle configuration with KCl-$MgCl_2$ molten salts mixture as high temperature fluid in the receiver, integrated with a Thermal Energy Storage system. The heliostat field performance and corresponding radiations maps on the receiver are derived through the simulation of a Gemasolar-type solar field. Three different sCO_2 cycle configurations were proposed and the most promising is the recompression with main compression intercooling (RMCI) cycle. With this sCO_2 cycle, the overall solar to electric efficiency was 24.46% determined at design condition and with an optimized TIT of 750 °C, which results from a compromise between cycle and receiver efficiency. A preliminary design of the turbine has been also carried out, leading to a three-stage configuration, thus demonstrating the technical feasibility of a machine with smaller weight and volume, lower complexity and thermal mass with respect to

Rankine steam cycle turbines. The yearly energy yield of the plant is 111.95 GWh, with a solar-to-electric efficiency of 18.38%. The obtained efficiency is comparable with the one estimated for a Gemasolar type power plant, based on Rankine cycle (18.8%): this result shows how the advantage achieved in the power cycle is counterbalanced by the poor receiver performance in particular at off-design conditions. The yearly average thermal efficiency for the high temperature HTF is equal to 63.9% which is 16.1 points percent lower than the one with conventional solar salts. The strong performance decay of the receiver for low incident radiation suggests a potential advantage on yearly basis of sCO_2 with lower TIT or solar fields with higher concentration ratios. Economic considerations were beyond the scope of this paper, nevertheless from an economic point of view, the cost savings on the power block [21] have to be compared with the increased cost of the receiver and of the TES. The similar solar-to-electric efficiency on yearly base of advanced solar tower with respect to commercial ones indicates that the adoption of high temperature molten salts with the current tower receiver design is probably not interesting for this technology. Future research activities should focus on the receiver design which must be modified or the adoption of another heat transfer fluid with better thermal properties. The limiting aspect of the molten salts in solar tower application is the low peak flux which can be withstood (1 MW/m^2) which limits the concentration ratio penalizing the thermal efficiency. This limit can be overcome by the adoption of other fluids with better thermal properties as liquid metals that could withstand twice the peak flux allowing theoretically for halved size receiver and thus halved thermal losses. Alternative solutions to enhance the overall efficiency can be the adoption of direct sCO_2 receivers, but in this case problems in terms of thermal storage arise.

Acknowledgements

The authors wish to thank Davide Castelli, Nicolò Lazzarin and Fabio Lo Mauro for their work on preliminary simulations carried out within their MSc thesis.

References

[1] IRENA. "Concentrating Solar Power,"; 2012.
[2] U.S.D. of Energy. "SunShot Vision Study,"; 2012.
[3] ASTRI. "Concentrating Solar Thermal TECHNOLOGIES Supporting the present – enabling the future Developing skills, capability and technology for leadership in the decarbonised energy future,"; 2016.
[4] Cohen GE, Kearney DW, Kolb GJ. "Final report on the operation and maintenance improvement program for concentrating solar power plants,"; 1999.
[5] ACCIONA. "Nevada Solar One." [Online]. Available: <http://www.acciona.us/projects/energy/concentrating-solar-power/nevada-solar-one/>. [accessed: 1-Jan-2017].
[6] Solar Millenium AG. "The parabolic trough power plants Andasol 1 to 3,"; 2008.
[7] Fernández-García A, Zarza E, Valenzuela L, Pérez M. Parabolic-trough solar collectors and their applications. Renew Sustain Energy Rev 2010;14(7):1695–721.
[8] Relloso S, Delgado E. "Experience with molten salt thermal storage in a commercial parabolic trough plant. Andasol-1 commissioning and operation. In: Proceedings of Solar paces conference; 2009.
[9] Giostri A, Binotti M, Astolfi M, Silva P, Macchi E, Manzolini G. Comparison of different solar plants based on parabolic trough technology. Sol. Energy 2012;86(5):1208–21.
[10] Manzolini G, Giostri A, Saccilotto C, Silva P, Macchi E. Development of an innovative code for the design of thermodynamic solar power plants part A: code description and test case. Renew Energy 2011;36(7):1993–2003.
[11] Giostri A, Binotti M, Silva P, Macchi E, Manzolini G. "Comparison of two linear collectors in solar thermal plants: parabolic trough versus Fresnel,". J Sol Energy Eng Trans ASME 2013;135(1).
[12] Morin G, Dersch J, Platzer W, Eck M, Häberle A. Comparison of linear fresnel and parabolic trough collector power plants. Sol Energy 2012;86(1):1–12.
[13] Giostri A, Binotti M, Silva P, Macchi E, Manzolini G. Comparison of two linear collectors in solar thermal plants: parabolic trough versus fresnel. J Sol Energy Eng 2012;135(1):11001.
[14] REN21. "RENEWABLES 2016, Global status report"; 2016.
[15] "sCO_2-hero.". Available: <http://www.sco2-hero.eu/>.
[16] Mecheri M, Le Moullec Y. Supercritical CO_2 Brayton cycles for coal-fired power plants. Energy 2016;103:758–71.
[17] Rochau GE. "Supercritical CO2 Brayton cycle. The DOE program". Supercritical CO_2 Power Cycle Symposium; 2011.
[18] NETL. "Supercritical carbon dioxide brayton cycle energy conversion R&D workshop", Leonardo Technologies Inc. (LTI) report under contract NETL DEFE0004002 - Task 300.02.09; Sept. 2014, Pittsburgh, USA.
[19] Musgrove G, Rimpel AM, Wilkes JC. Fundamentals of supercritical CO_2. Supercritical CO2 Power Cycle Symposium; 2016. p. 110.
[20] Angelino G. Real gas effects in carbon dioxide cycles", no. ASME Paper No. 69-GT-103; 1969.
[21] Dostal V, Driscoll MJ, Hejzlar P. Advanced nuclear power technology program a supercritical carbon dioxide cycle for next generation nuclear reactors; 2004.
[22] Ahn Y, Bae SJ, Kim M, Cho SK, Baik S, Lee JI, et al. Review of supercritical CO_2 power cycle technology and current status of research and development. Nucl Eng Technol 2015;47(6):647–61.
[23] Crespi F, Gavagnin G, Sánchez D, Martínez GS. Supercritical carbon dioxide cycles for power generation: a review. Appl Energy 2017;195:152–83.
[24] Wang K, He Y-L, Zhu H-H. Integration between supercritical CO_2 Brayton cycles and molten salt solar power towers: a review and a comprehensive comparison of different cycle layouts. Appl Energy 2017;195:819–36.
[25] Bauer ML, Vijaykumar R, Lausten M, Stekli J. Pathways to cost competitive concentrated solar power incorporating supercritical carbon dioxide power cycles. In: The 5th international symposium; 2016.
[26] Iverson BD, Conboy TM, Pasch JJ, Kruizenga AM. Supercritical CO_2 Brayton cycles for solar-thermal energy. Appl Energy 2013;111:957–70.
[27] Turchi W, Ma Z, Neises T. Thermodynamic study of advanced supercritical carbon dioxide power cycles for high performance concentrating solar power systems. J Sol Energy Eng 2013;135(4):41007.
[28] Garg P, Kumar P, Srinivasan K. Supercritical carbon dioxide Brayton cycle for concentrated solar power. J Supercrit Fluids 2013;76:54–60.
[29] Casella F, Colonna P. Development of a modelica dynamic model of solar supercritical CO_2 brayton cycle power plants for control studies. In: Proceedings of the supercritical CO_2 power cycle symposium; 2011.
[30] Singh R, Rowlands AS, Miller SA. Effects of relative volume-ratios on dynamic performance of a direct-heated supercritical carbon-dioxide closed Brayton cycle in a solar-thermal power plant. Energy 2013;55:1025–32.
[31] Cao G, Firouzdor V, Sridharan K, Anderson M, Allen TR. Corrosion of austenitic alloys in high temperature supercritical carbon dioxide. Corros Sci 2012;60:246–55.
[32] Moore R, Conboy T. Metal corrosion in a supercritical carbon dioxide-liquid sodium power cycle. NM: Albuquerque; 2012.
[33] Besarati SM, Yogi Goswami D. "Analysis of advanced supercritical carbon dioxide power cycles with a bottoming cycle for concentrating solar power applications". J Sol Energy Eng; 2013.
[34] Lemmon EW, Huber ML, McLinden MO. NIST standard reference database 23: reference fluid thermodynamic and transport properties-REFPROP, Version 9.1. Gaithersburg: National Institute of Standards and Technology; 2013.
[35] Monge Brenes B. Design of supercritical carbon dioxide centrifugal compressors; 2014.
[36] Musgrove GO, Le Pierres R, Nash J. "Heat exhangers for supercritical CO2 power cycle applications. In: The 4th international symposium for supercritical CO_2 power cycles; 2014.
[37] Wright SA, Radel RF, Vernon ME, Rochau GE, Pickard PS. "Operation and analysis of a supercritical CO_2 brayton cycle"; 2010.
[38] Fourspring PM, Nehrbauer JP, Sullivan S, Nash J. Testing of compact recuperators for a supercritical CO2 Brayton power cycle. In: Proceedings of the 4th international symposium on supercritical CO_2 power cycles; 2014.
[39] LUVE, "Air Cooled Condensers." [Online]. Available: <http://manuals.luve.it/Air-Cooled-Condensers/files/assets/common/downloads/page0021.pdf> [accessed: 15-Apr-2017].
[40] "Private communication with LU.VE"; 2016.
[41] HEATRIC, "Heat Exchangers | Heatric | PCHE Specialists." [Online]. Available: <http://www.heatric.com/diffusion_bonded_heat_exchangers.html> [accessed: 29-Jan-2017].
[42] Macchi E, Astolfi M. "9 – Axial flow turbines for Organic Rankine Cycle applications". In: Organic rankine cycle (ORC) power systems; 2017. p. 299–319.
[43] Astolfi M, Binotti M, Mazzola S, Zanellato L, Manzolini G. Heliostat aiming point optimization for external tower receiver. Sol Energy 2016. http://dx.doi.org/10.1016/j.solener.2016.03.042 Apr.
[44] Rinaldi F, Binotti M, Giostri A, Manzolini G. Comparison of linear and point focus collectors in solar power plants. Energy Proc 2013;49:1491–500.
[45] Binotti M, De Giorgi P, Sanchez D, Manzolini G. Comparison of different strategies for heliostats aiming point in cavity and external tower receivers. J Sol Energy Eng 2016;138(2):21008.
[46] Kistler B. "Auser's manual for DELSOL3: a computer code for calculating the optical performance and optimal system design for solar thermal central receiver plants."; 1986.
[47] Williams DF. Assessment of Candidate Molten Salt Coolants for the NGNP/NHI Heat-Transfer Loop"; 2006.
[48] Castelli D. "Development of a thermal model for a solar tower receiver using single phase heat trasnfer fluid (in Italian)". Politecnico di Milano; 2014.
[49] Rodríguez-Sánchez MR, Marugan-Cruz C, Acosta-Iborra A, Santana D. Comparison of simplified heat transfer models and CFD simulations for molten salt external receiver. Appl Therm Eng Sep. 2014;73:991–1003.

[50] Siebers D, Kraabel J. Estimating convective energy losses from solar central receivers; 1984.
[51] Rodríguez-Sánchez MR, Marugan-Cruz C, Acosta-Iborra A, Santana D. Comparison of simplified heat transfer models and CFD simulations for molten salt external receiver. Appl Therm Eng Dec. 2014;73(1):993–1005.
[52] Pacheco J. Final test and evaluation results from the solar two project. NM, US: Albuquerque; 2002.
[53] Rodríguez-Sánchez MR, Soria-Verdugo A, Almendros-Ibáñez JA, Acosta-Iborra A, Santana D. Thermal design guidelines of solar power towers. Appl Therm Eng Feb. 2014;63(1):428–38.
[54] Macchi E, Perdichizzi A. Efficiency prediction for axial-flow turbines operating with nonconventional fluids. J Eng Gas Turbine Power 1981;103(4):718–24.
[55] Craig HR, Cox HJA. Performance estimation of axial flow turbines. In: Proceedings of the institution of mechanical engineers. pp. 407–423, https://doi.org/10.1243/PIME_PROC_1970_185_048_02.
[56] Kacker SC, Okapuu U. A mean line prediction method for axial flow turbine efficiency. J Eng Power 1982;104(1):111.
[57] ''ENERGY plus,'' U.S. Department of Energy's (DOE) Building Technologies Office (BTO), and managed by the National Renewable Energy Laboratory (NREL). [Online]. Available: <https://energyplus.net/>.
[58] Binotti M, Manzolini G, Zhu G. An alternative methodology to treat solar radiation data for the optical efficiency estimate of different types of collectors. Sol Energy 2014;110:807–17.
[59] Lazzarin F, Lo Mauro N. ''Techno-economic simulation and analisys of supercritical CO_2 cycles for solar tower plants with thermal energy storage (in Italian)''. Politecnico di Milano; 2015.
[60] Falcone PK. A handbook for solar central receiver design. Albuquerque, NM, and Livermore, CA (United States); Dec. 1986.